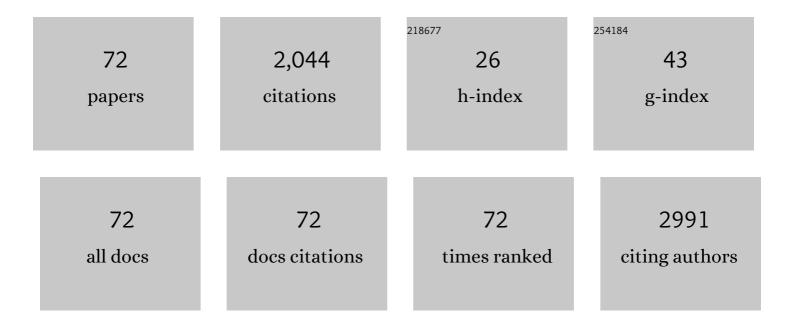
Chuncai Kong

List of Publications by Year in descending order

Source: https://exaly.com/author-pdf/5814880/publications.pdf Version: 2024-02-01



#	Article	IF	CITATIONS
1	Yolk–Shell Cu ₂ O@CuOâ€decorated RGO for Highâ€Performance Lithium″on Battery Anode. Energy and Environmental Materials, 2022, 5, 253-260.	12.8	37
2	Cu2O-based binary and ternary photocatalysts for the degradation of organic dyes under visible light. Ceramics International, 2022, 48, 1757-1764.	4.8	10
3	Caterpillar-like Ag–ZnO–C hollow nanocomposites for efficient solar photocatalytic degradation and disinfection. Environmental Science: Nano, 2022, 9, 975-987.	4.3	2
4	Enhancement of energy storage properties of Bi0.5Na0.5TiO3-based relaxor ferroelectric under moderate electric field. Applied Physics Letters, 2022, 120, .	3.3	5
5	Geometries, electronic structures, and bonding properties of endohedral Groupâ€14 Zintl clusters <scp>TM</scp> @ <scp>E₁₀</scp> (<scp>TM</scp> = Fe, Co, Ni; E = Ge, Sn, Pb). Journal of Computational Chemistry, 2022, 43, 828-838.	3.3	3
6	Inter-embedded Au-Cu2O heterostructure for the enhanced hydrogen production from water splitting under the visible light. Chemical Engineering Journal, 2021, 405, 126709.	12.7	27
7	Stabilities, Electronic Structures, and Bonding Properties of 20-Electron Transition Metal Complexes (Cp) ₂ TMO and their One-Dimensional Sandwich Molecular Wires (Cp =) Tj ETQq1 1 0.784314 rgBT	/Overlock 2.5	10 Tf 50 50. 2
8	125, 721-730. Ultrafine RhNi Nanocatalysts Confined in Hollow Mesoporous Carbons for a Highly Efficient Hydrogen Production from Ammonia Borane. Inorganic Chemistry, 2021, 60, 6820-6828.	4.0	31
9	Novel Design of 3-D Microstructure Contact Material Generating Autoexcitation Magnetic Field. IEEE Transactions on Plasma Science, 2021, 49, 1969-1974.	1.3	Ο
10	RGO@Cu2O@Cu Ternary Nanocomposite for High-Performance Non-Enzymatic Glucose Detection. Journal of the Electrochemical Society, 2021, 168, 087503.	2.9	6
11	Manipulating Cu Nanoparticle Surface Oxidation States Tunes Catalytic Selectivity toward CH ₄ or C ₂₊ Products in CO ₂ Electroreduction. Advanced Energy Materials, 2021, 11, 2101424.	19.5	71
12	Theoretical Insight into 20â€Electron Transition Metal Complexes (C ₅ H ₅) ₂ TM(E ₁ E ₂) ₂ (TM =â€ Bonding Nature. Physica Status Solidi (B): Basic Research, 2021, 258, 2100417.	‰Cr,) Tj E 1.5,) Tj E	TQq0 0 0 rgl
13	CoFe Nanoparticle-Decorated Reduced Graphene Oxide for the Highly Efficient Reduction of 4-Nitrophenol. Langmuir, 2021, 37, 10987-10993.	3.5	8
14	Manipulating Cu Nanoparticle Surface Oxidation States Tunes Catalytic Selectivity toward CH ₄ or C ₂₊ Products in CO ₂ Electroreduction (Adv. Energy) Tj ETQq0 0 () r g₿Љ /Ov	erløck 10 Tf S
15	Stable Noble Gas Compounds Based on Superelectrophilic Anions [B ₁₂ (BO) ₁₁] ^{â^'} and [B ₁₂ (OBO) ₁₁] ^{â^'} . ChemPhysChem, 2021, 22, 2240-2246.	2.1	5
16	Designing stable <i>closo</i> -B ₁₂ dianions <i>in silico</i> for Li- and Mg-ion battery applications. Inorganic Chemistry Frontiers, 2021, 8, 5201-5208.	6.0	0
17	Endohedral group-14-element clusters TM@E ₉ (TM = Co, Ni, Cu; E = Ge, Sn, Pb) and their low-dimensional nanostructures: a first-principles study. Physical Chemistry Chemical Physics, 2021, 23, 20654-20665.	2.8	6
18	Atomically ordered Rh ₂ P catalysts anchored within hollow mesoporous carbon for efficient hydrogen production. Chemical Communications, 2021, 57, 12345-12348.	4.1	11

CHUNCAI KONG

#	Article	IF	CITATIONS
19	Reaction mechanism, norbornene and ligand effects, and origins of meta-selectivity of Pd/norbornene-catalyzed C–H activation. Chemical Science, 2020, 11, 113-125.	7.4	11
20	Ag nanoparticles decorated PVA-co-PE nanofiber-based membrane with antifouling surface for highly efficient inactivation and interception of bacteria. Applied Surface Science, 2020, 506, 144664.	6.1	32
21	Polymeric Ligand-Mediated Regioselective Bonding of Plasmonic Nanoplates and Nanospheres. Journal of the American Chemical Society, 2020, 142, 17282-17286.	13.7	25
22	Stabilities, Electronic Structures, and Bonding Properties of Iron Complexes (E 1 E 2)Fe(CO) 2 (CNAr) Tj ETQq0	0 0 rgBT /(1.9	Overlock 10 T
23	Synthesis and Crystal-Phase Engineering of Mesoporous Palladium–Boron Alloy Nanoparticles. ACS Central Science, 2020, 6, 2347-2353.	11.3	36
24	Template-assisted synthesis of CuO hollow nanotubes constructed by ultrathin nanosheets for lithium-ion battery applications. Journal of Alloys and Compounds, 2020, 849, 156635.	5.5	34
25	2D hydrogenated boride as a reductant and stabilizer for <i>in situ</i> synthesis of ultrafine and surfactant-free carbon supported noble metal electrocatalysts with enhanced activity and stability. Journal of Materials Chemistry A, 2020, 8, 18856-18862.	10.3	11
26	Low-Cost Synthetic Honeycomb-like Carbon Derived from Cotton as a Sulfur Host for the Enhanced Electrochemical Performances of Lithium–Sulfur Batteries. Energy & Fuels, 2020, 34, 13096-13103.	5.1	8
27	Boosting areal energy density of 3D printed all-solid-state flexible microsupercapacitors via tailoring graphene composition. Energy Storage Materials, 2020, 30, 412-419.	18.0	38
28	Intrinsic insight on localized surface plasmon resonance enhanced methanol electro-oxidation over a Au@AgPt hollow urchin-like nanostructure. Journal of Materials Chemistry A, 2020, 8, 6638-6646.	10.3	19
29	An Mn ²⁺ -mediated construction of rhombicuboctahedral Cu ₂ O nanocrystals enclosed by jagged surfaces for enhanced enzyme-free glucose sensing. CrystEngComm, 2020, 22, 2042-2048.	2.6	11
30	Cu–Cu ₂ 0 Heterogeneous Architecture for the Enhanced CO Catalytic Oxidation. Advanced Materials Interfaces, 2020, 7, 1901643.	3.7	17
31	Ultrathin CuxO nanoflakes anchored Cu2O nanoarray for high-performance non-enzymatic glucose sensor. Journal of Solid State Electrochemistry, 2020, 24, 583-590.	2.5	6
32	Synthesis of porous carbon nano-onions derived from rice husk for high-performance supercapacitors. Applied Surface Science, 2019, 488, 593-599.	6.1	57
33	CuO ultrathin nanosheets decorated reduced graphene oxide as a high performance anode for lithium-ion batteries. Journal of Alloys and Compounds, 2019, 805, 355-362.	5.5	27

34	Wearable, stable, highly sensitive hydrogel–graphene strain sensors. Beilstein Journal of Nanotechnology, 2019, 10, 475-480.	2.8	38
35	Localized surface plasmon enhanced electrocatalytic methanol oxidation of AgPt bimetallic nanoparticles with an ultra-thin shell. Chemical Communications, 2019, 55, 3943-3946.	4.1	24

³⁶A Readily Accessible Functional Nanofibrous Membrane for Highâ€Capacity Immobilization of Ag
Nanoparticles and Ultrafast Catalysis Application. Advanced Materials Interfaces, 2019, 6, 1801617.3.715

Chuncai Kong

#	Article	IF	CITATIONS
37	One-pot synthesis of ultrafine Ag-hydrogel composites with enhanced catalytic reduction of 4-nitrophenol. Materials Letters, 2019, 236, 530-533.	2.6	10
38	Templated-synthesis of hierarchical Ag-AgBr hollow cubes with enhanced visible-light-responsive photocatalytic activity. Applied Surface Science, 2018, 443, 492-496.	6.1	14
39	A sensitive electrochemical nonenzymatic biosensor for the detection of H2O2 released from living cells based on ultrathin concave Ag nanosheets. Biosensors and Bioelectronics, 2018, 106, 29-36.	10.1	88
40	Template-synthesis of hierarchical CuO nanoflowers constructed by ultrathin nanosheets and their application for non-enzymatic glucose detection. Materials Letters, 2018, 219, 134-137.	2.6	27
41	Immobilized Seed-Mediated Growth of Two-Dimensional Array of Metallic Nanocrystals with Asymmetric Shapes. ACS Nano, 2018, 12, 1107-1119.	14.6	18
42	Nanosized nickel decorated sisal fibers with tailored aggregation structures for catalysis reduction of toxic aromatic compounds. Industrial Crops and Products, 2018, 119, 226-236.	5.2	4
43	Cooperative Assembly of Magneto-Nanovesicles with Tunable Wall Thickness and Permeability for MRI-Guided Drug Delivery. Journal of the American Chemical Society, 2018, 140, 4666-4677.	13.7	138
44	Sweat-based wearable energy harvesting-storage hybrid textile devices. Energy and Environmental Science, 2018, 11, 3431-3442.	30.8	196
45	Controllable inâ€situ Synthesis of Cu–Cu ₂ O Heterostructures with Enhanced Visibleâ€kight Photocatalytic Activity. ChemistrySelect, 2018, 3, 10641-10645.	1.5	13
46	Continuous UV irradiation synthesis of ultra-small Au nanoparticles decorated Cu2O with enhanced photocatalytic activity. Composites Communications, 2018, 9, 27-32.	6.3	6
47	Surfactant-free synthesis of Cu ₂ O yolk–shell cubes decorated with Pt nanoparticles for enhanced H ₂ O ₂ detection. Chemical Communications, 2018, 54, 8458-8461.	4.1	36
48	Facile synthesis of novel CuO/Cu2O nanosheets on copper foil for high sensitive nonenzymatic glucose biosensor. Sensors and Actuators B: Chemical, 2017, 248, 630-638.	7.8	113
49	Zinc ion mediated synthesis of cuprous oxide crystals for non-enzymatic glucose detection. Journal of Materials Chemistry B, 2017, 5, 8686-8694.	5.8	21
50	Modified thermal resistance networks model for transverse thermal conductivity of unidirectional fiber composite. Composites Communications, 2017, 6, 52-58.	6.3	12
51	Facet-dependent nonenzymatic glucose sensing properties of Cu ₂ O cubes and octahedra. New Journal of Chemistry, 2016, 40, 6573-6576.	2.8	35
52	One-pot synthesis of etched Cu ₂ O cubes with exposed {110} facets with enhanced visible-light-driven photocatalytic activity. Physical Chemistry Chemical Physics, 2015, 17, 29479-29482.	2.8	18
53	Facile hydroxyl-assisted synthesis of morphological Cu ₂ O architectures and their shape-dependent photocatalytic performances. New Journal of Chemistry, 2014, 38, 4656-4660.	2.8	30
54	Copper-templated synthesis of gold microcages for sensitive surface-enhanced Raman scattering activity. RSC Advances, 2014, 4, 27074-27077.	3.6	7

Chuncai Kong

#	Article	IF	CITATIONS
55	Nanoparticle-aggregated CuO nanoellipsoids for high-performance non-enzymatic glucose detection. Journal of Materials Chemistry A, 2014, 2, 10073.	10.3	80
56	Templating synthesis of hollow CuO polyhedron and its application for nonenzymatic glucose detection. Journal of Materials Chemistry A, 2014, 2, 7306-7312.	10.3	87
57	Nanoparticle-aggregated hollow copper microcages and their surface-enhanced Raman scattering activity. CrystEngComm, 2013, 15, 6136.	2.6	23
58	Twins in polyhedral 26-facet Cu7S4 cages: Synthesis, characterization and their enhancing photochemical activities. Dalton Transactions, 2012, 41, 3214.	3.3	35
59	Copper sulfide cages wholly exposed with nanotwinned building blocks. CrystEngComm, 2012, 14, 67-70.	2.6	34
60	Facet-selective growth of Cu–Cu ₂ O heterogeneous architectures. CrystEngComm, 2012, 14, 40-43.	2.6	54
61	Nanocube-aggregated cauliflower-like copper hierarchical architectures: synthesis, growth mechanism and electrocatalytic activity. CrystEngComm, 2012, 14, 5737.	2.6	16
62	Magnetic field driven assembly of 1D-aligned silver superstructures. CrystEngComm, 2011, 13, 4827.	2.6	8
63	Nanoparticle-aggregated octahedral copper hierarchical nanostructures. CrystEngComm, 2011, 13, 63-66.	2.6	16
64	Polyhedron-aggregated multi-facet Cu2O homogeneous structures. CrystEngComm, 2011, 13, 6040.	2.6	22
65	Unique polyhedral 26-facet CuS hollow architectures decorated with nanotwinned, mesostructural and single crystalline shells. CrystEngComm, 2011, 13, 6200.	2.6	39
66	Nanoparticle-aggregated paddy-like copper dendritic nanostructures. CrystEngComm, 2011, 13, 1916-1921.	2.6	23
67	Selective-etching growth of urchin-like Cu2O architectures. CrystEngComm, 2011, 13, 6616.	2.6	31
68	Etching-limited branching growth of cuprous oxide during ethanol-assisted solution synthesis. CrystEngComm, 2011, 13, 2837.	2.6	39
69	Seed-mediated synthesis of polyhedral 50-facet Cu2O architectures. CrystEngComm, 2011, 13, 5993.	2.6	29
70	Highly symmetric polyhedral Cu2O crystals with controllable-index planes. CrystEngComm, 2011, 13, 2217.	2.6	75
71	Designated-Tailoring on {100} Facets of Cu ₂ O Nanostructures: From Octahedral to Its Different Truncated Forms. Journal of Nanomaterials, 2010, 2010, 1-11.	2.7	8
72	Rapid Oxidation Synthesis of Hollow Cupric Oxide-Decorated rGO with High Performance and Kinetically Enhanced Lithium Storage. Energy & Fuels, 0, , .	5.1	1